Supplemental Material:

NMR Evidence for Universal Pseudogap Behavior in Quasi-Two-Dimensional FeSe-Based Superconductors

B. L. Kang(康宝蕾)[1,†], M. Z. Shi(石孟竹)[1,†], D. Zhao(赵丹)[1], S. J. Li(李顺姣)[1], J. Li(李建)[1], L. X. Zheng(郑立玄)[1], D. W. Song(宋殿武)[1], L. P. Nie(聂林鹏)[1], T. Wu(吴涛)[1,2,3,4,5*], and X. H. Chen(陈仙辉)[1,2,3,4,5*]

[1]*Hefei National Research Center for Physical Sciences at the Microscale, University of Science and Technology of China, Hefei, Anhui 230026, China*

[2]*Key Laboratory of Strongly coupled Quantum Matter Physics, Department of Physics, University of Science and Technology of China, Hefei, Anhui 230026, China*

[3]*CAS Center for Excellence in Superconducting Electronics (CENSE), Shanghai 200050, China*

[4]*Collaborative Innovation Center of Advanced Microstructures, Nanjing University, Nanjing 210093, China*

[5]*Hefei National Laboratory, University of Science and Technology of China, Hefei 230088, China*

*Corresponding author. Email: wutao@ustc.edu.cn; chenxh@ustc.edu.cn

†These authors contributed equally to this work

1. Experimental Methods

Crystal growth of $(PY)_xFeSe$. $(PY)_xFeSe$ is synthesized through an electrochemical intercalation process using an FeSe single crystal as the starting material. The process is analogous to that of $(CTA)_xFeSe$ [1] and $(TBA)_xFeSe$ [2]. First, high-quality single crystals of tetragonal FeSe were grown using a KCl-$AlCl_3$ flux method [3]. Second, the weighted FeSe single crystal (~1 mg) is fixed onto an indium wire as the positive electrode, while a silver piece is used as the negative electrode. The electrolyte was obtained by dissolving 0.5 g PY (1-butyl-1-methylpyrrolidinium bromide, TCI, 97%) into 10 ml DMF (N,N-dimethylformamide, Innochem, 99.9%, extra dry with molecular sieves, water less than 50 ppm). The electrochemical intercalation process was controlled by a Lanhe testing system, and here, a constant current of 10 μA was applied. During the current passing through the electrolytic cell, the negative electrode loses electrons, while the

positive electrode obtains electrons. The doping amount x in $(PY)_xFeSe$ is controlled by adjusting the charge passing through the electrolytic cell based on the Faraday law. For a fixed doping amount x, the time t needed can be calculated using the formula $t = Fmx/MI$, where t is the time of the galvanostatic discharge process, F is the Faraday constant (96485.31 C mol^{-1}), m is the mass (g) of the pristine FeSe single crystal, x is the amount of intercalated PY ions, M is the molar mass of FeSe (134.805 g mol^{-1}), and I is the electrical current (A) passing through the cell. In this case, x is set as 1 to achieve uniform and single-phase intercalation. All processes were handled in an argon-filled glove box. The resulting $(PY)_xFeSe$ single crystal maintains a plate-like morphology yet is much thicker.

XRD phase identification and composition analysis. The X-ray diffraction pattern of the sample was collected on a Rigaku SmartLab-9 powder diffractometer with Cu Kα radiation. The composition and actual doping level x in $(PY)_xFeSe$ were determined using an electron probe X-ray microanalyzer (EPMA-8050G, Shimadzu). High-sensitivity qualitative and quantitative elemental analyses, together with element mapping, were applied.

Magnetic and electrical transport measurements. Magnetic susceptibility was measured employing the commercial SQUID-VSM (7 T, Quantum Design). The magnetization was measured in FC and ZFC modes under a magnetic field of 5 Oe. The electrical transport measurements were performed with a Physical Property Measurement System (PPMS-9 T, Quantum Design) by a standard *dc* four-probe method. Considering the air sensitivity of $(PY)_xFeSe$, all the preparation processes for characterization and measurement were handled in an argon-filled glove box, and the samples were coated with a thin layer of chemically stable high-vacuum silicone grease before being taken outside the glove box.

Nuclear magnetic resonance measurements. The standard NMR spin–echo technique was applied using a commercial NMR spectrometer from Thamway Co. Ltd. The external magnetic field was generated by a 12 T magnet from Oxford Instruments. The ^{63}Cu NMR signal from the copper coil was used to calibrate the external field. ^{77}Se NMR spectra were obtained by the fast Fourier transform (FFT) method. The nuclei of ^{77}Se have a nuclear spin $I = 1/2$, and the Knight shift was extracted from the NMR central transition line using the gyromagnetic ratio $\gamma/2\pi = 8.118$ MHz/T. The ^{77}Se spin-lattice relaxation time (T_1) measurements were carried out by using the saturation-recovery method at the peak positions of NMR spectra at all temperatures, and the

spin–echo decay was fitted by a simple exponential function $m(t) = A_0+Aexp[-(t/T_1)^r]$. Error bars are determined by least square fitting to the experimental data.

2. Supplemental Figures and captions

The XRD patterns for pristine FeSe and intercalated $(PY)_x$FeSe single crystals are shown in Fig. S1.

Figure S2 shows the high-sensitivity EPMA measurement for $(PY)_x$FeSe.

Figure S3 shows the superconducting property for $(PY)_x$FeSe.

Figure S4 offers supplementary information about the NMR measurement for $(PY)_x$FeSe, including the tuning frequency of the NMR coil, the spectra of ^{77}Se nuclei and the temperature evolution of the stretching exponent *r*.

Figure S5 plots the temperature dependence of the Knight shift and $1/T_1T$ for $(PY)_x$FeSe, with an external magnetic field of 12 T being applied in plane and out of plane.

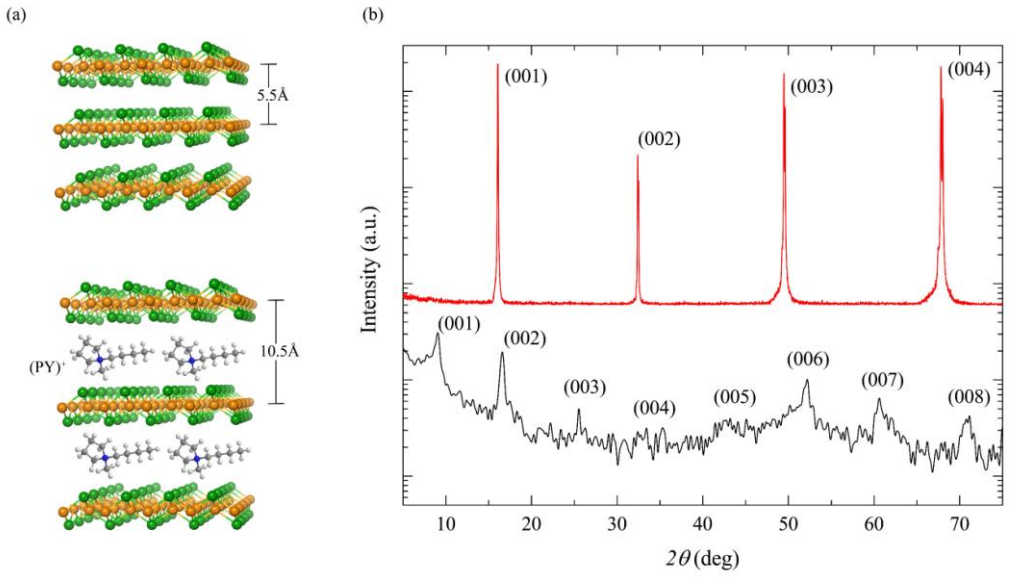

FIG. S1. (a) Crystal structures of pristine FeSe and $(PY)_x$FeSe. The distance between adjacent FeSe layers greatly increased from 5.5 Å to 10.5 Å through the intercalation of PY^+. (b) XRD patterns for FeSe and $(PY)_x$FeSe single crystals. The (00 l) reflections are well indexed.

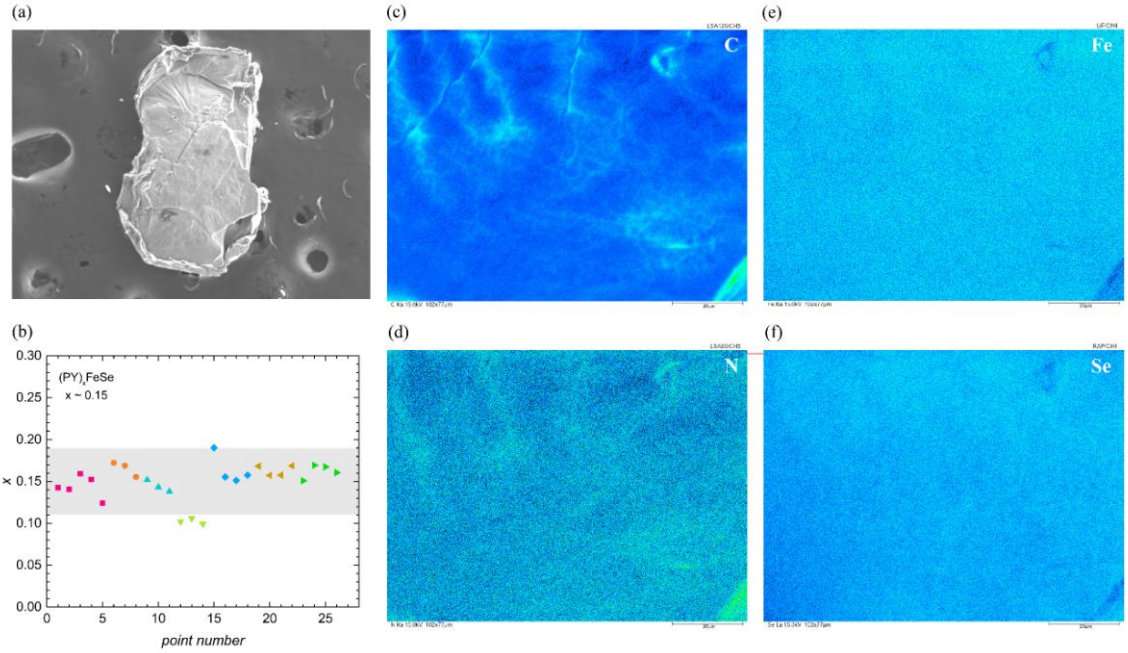

FIG. S2. (a) High-resolution SEM image of a freshly cleaved surface of $(PY)_xFeSe$. (b) Quantitative analysis of the doping level x for $(PY)_xFeSe$. The points labeled in the same color are from different locations of one sample. (c-f) High-definition element mapping analysis in a 102×77 μm area for the main composition elements, including C, N, Fe and Se.

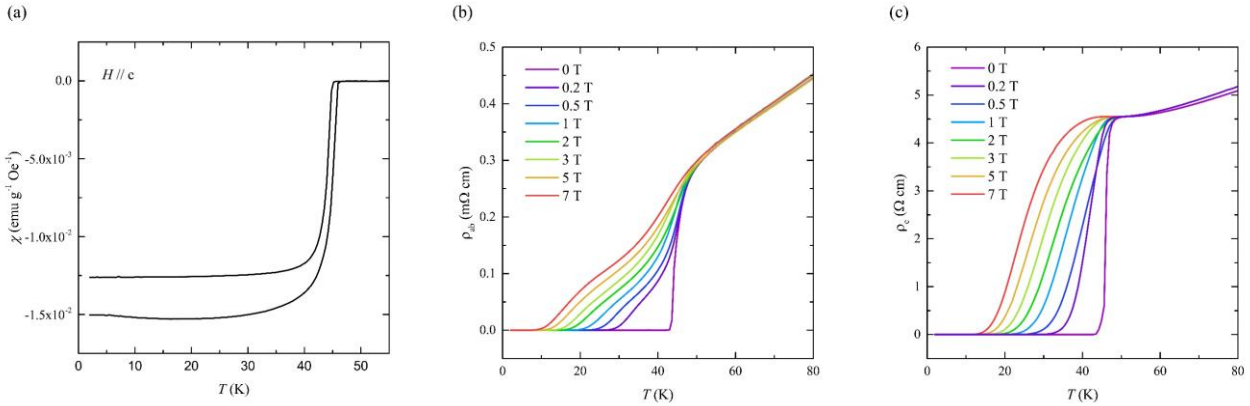

FIG. S3. (a) Temperature dependence of magnetic susceptibility measured in FC and ZFC modes under a magnetic field of 5 Oe. (b) The temperature dependence of the in-plane resistivity under different magnetic fields applied along the c axis. The fan-shaped broadening under magnetic fields indicates a strong 2D characteristic. (c) Temperature dependence of the out-of-plane resistivity under different magnetic fields applied along the c axis.

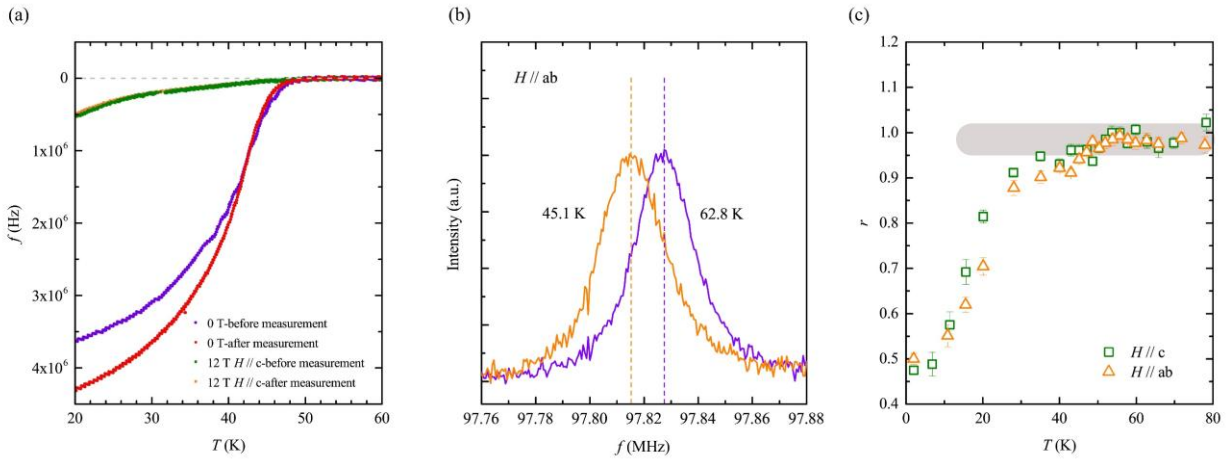

FIG. S4. (a) Tuning frequency of the NMR coil before and after the NMR measurements. The frequency shift indicates a clear superconducting transition. (b) NMR spectra of ^{77}Se nuclei measured at 45.1 K and 62.8 K, respectively. The uniform frequency shift of the NMR spectrum without obvious distortion or broadening indicates an intrinsic change in the Knight shift below T_p. (c) Temperature evolution of the stretching exponent r. The value of r is extracted from the T_1 fitting by the stretched exponential function. It remains nearly constant in the temperature range between T_{c0} and T_p.

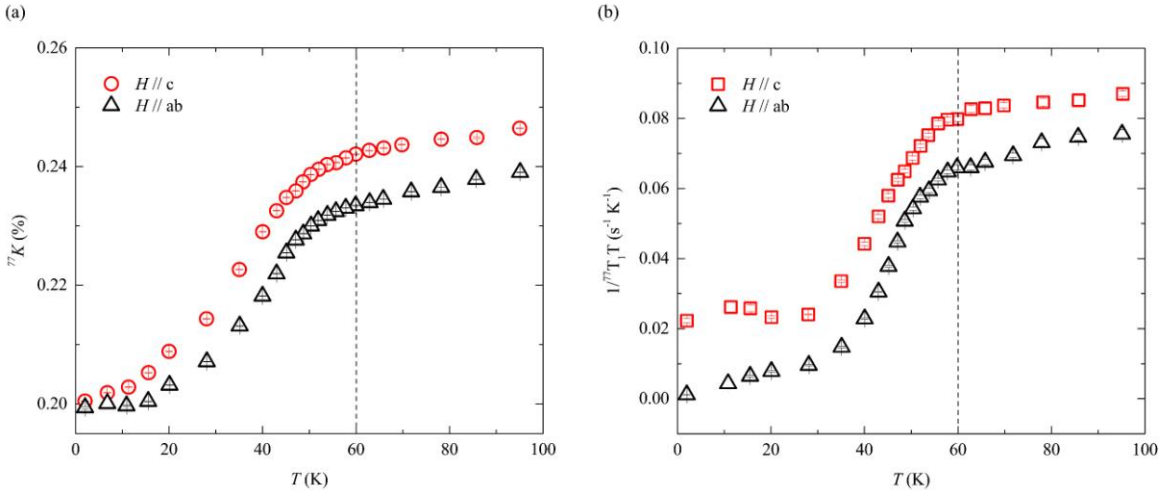

FIG. S5. (a) Temperature dependence of the Knight shift for $(PY)_xFeSe$. (b) Temperature dependence of the spin-lattice relaxation rate divided by temperature $1/T_1T$ for $(PY)_xFeSe$. The external magnetic field is 12 T in (a) and (b). The vertical dashed lines at ~ 60 K indicate the onset temperature of local superconducting pairing.

.

Reference:

[1] M. Z. Shi, N. Z. Wang, B. Lei, C. Shang, F. B. Meng, L. K. Ma, F. X. Zhang, D. Z. Kuang, and X. H. Chen, Phys. Rev. Mater. 2, 074801 (2018).

[2] M. Z. Shi, N. Z. Wang, B. Lei, J. J. Ying, C. S. Zhu, Z. L. Sun, J. H. Cui, F. B. Meng, C. Shang, L. K. Ma, and X. H. Chen, New J. Phys. 20, 123007 (2018).

[3] D. Chareev, E. Osadchii, T. Kuzmicheva, J. Y. Lin, S. Kuzmichev, O. Volkova, and A. Vasiliev, CrystEngComm 15, 1989 (2013).